Advances in Forest Fire Research 2018

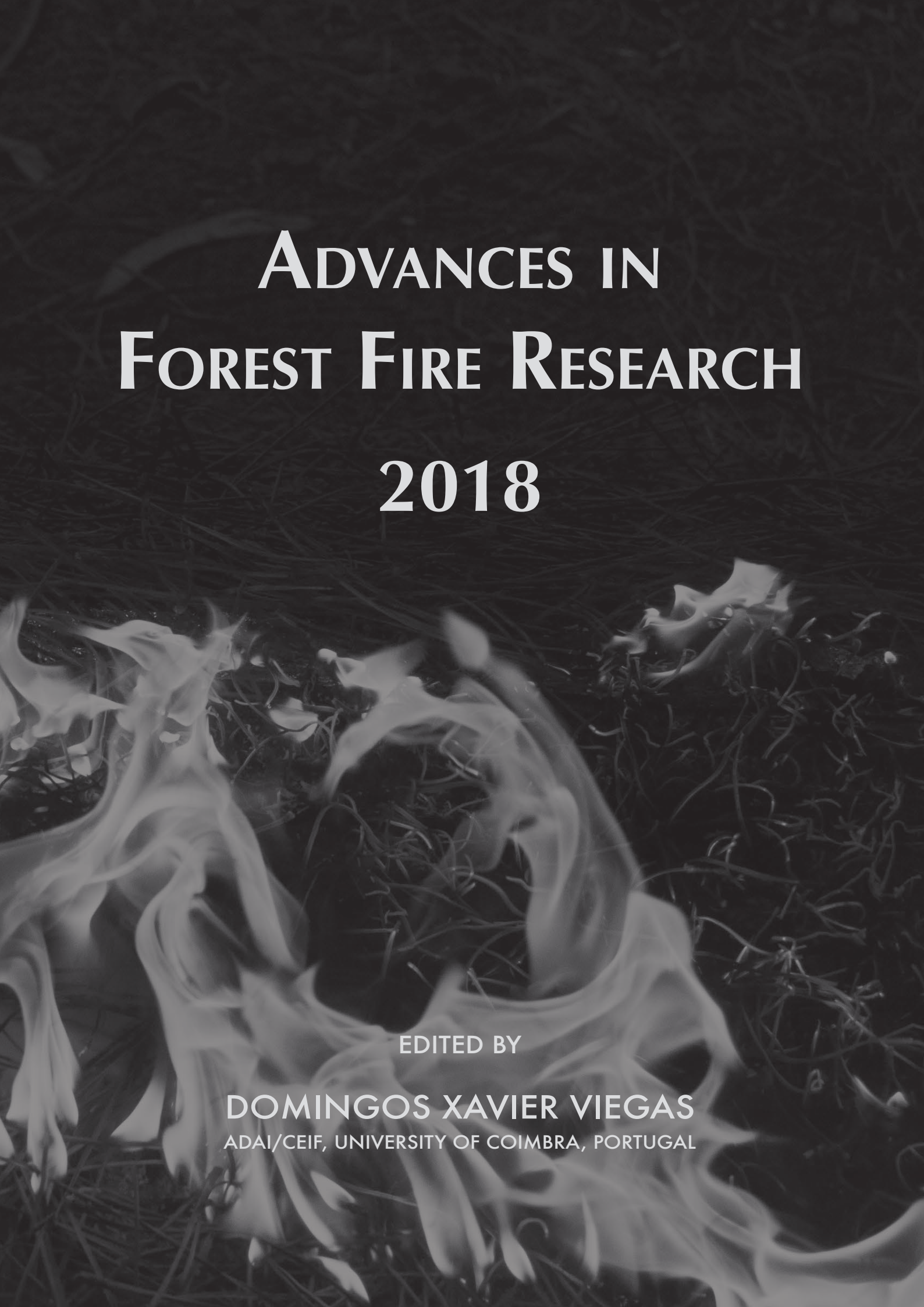

EDITED BY

DOMINGOS XAVIER VIEGAS

ADAI/CEIF, UNIVERSITY OF COIMBRA, PORTUGAL

https://doi.org/10.14195/978-989-26-16-506_75

The role of the terrain-modified wind on driving the fire behaviour over hills – an Experimental and Numerical Analysis.

Abdelrahman Abouali*; Jorge Rafael Raposo; Domingos Xavier Viegas
Forest Fire Research Centre (CEIF), ADAI–LAETA, University of Coimbra, 3030 - 289 Coimbra, Portugal. {abouali@adai.pt}*

Abstract

This paper analyses the fire behaviour over two hills placed in series in the direction of the wind. Laboratory-scale experiments under various slope and wind velocity conditions with changing the distance between the hills revealed two sorts of extreme fire behaviour that might take place. One is a lateral fire spread over the lee slopes (fire channelling), and the other is an eruptive fire behaviour (blow-up) happens over the windward face of the secondly ordered hill in the direction of the wind. The changes in the blowing wind velocity and the distance between the hills were found to have a significant effect on fire behaviours, where increasing the wind speed or the distance resulted in a faster rate of spread of the fire. Also, the change of the ignition point, or spreading direction of the fire relatively to the wind direction has a significant effect on the fire channelling behaviour where it was found that the fire channelling is more extreme if the fire is spreading against the main wind direction. Numerical analysis of the adiabatic flow field showed that the change the presence of these extreme fire behaviour is related directly to the terrain-modified flow topology. The interactions between the terrain-modified wind mechanisms and the fire result in accelerated flows that drive the indicated extreme fire behaviours.

Keywords: Fire channelling, lateral fire spread, fire over slopes, fire-induced wind, eruptive fire, fire blow-up

1. Introduction

Wildfire behaviour has caught the attention of wildfire researchers during the last decade to understand how the fire is behaving under certain conditions in order to better predict the wildfire evolution. Identifying the conditions where an extreme fire behaviour (Viegas 2004) may take place is crucial for the safety of the firefighting teams and the wildland-urban-interface (WUI) communities. The wind, complex terrain and their interactions are common conditions that may lead to extreme fire behaviour. Many numerical and experimental studies were carried out to analyse the fire behaviour over the complex terrains namely on slopes and hills. However, we still lack understanding on the behaviour of fire spreading over complex terrains, namely the effect of having other topographic obstacles around the topography of interest (i.e. the topography that the fire propagates over it). In this paper, we are investigating the fire behaviour over hills ordered in series in the direction of the wind. This configuration is closer to the existence of hills in nature, where the hills are rarely found isolated as the configuration that was investigated on the previously mentioned studies.

Previous studies (McRae 2004; Sharples *et al.* 2012) showed that, for a fire spreading over the leeward face of a hill with the wind blowing perpendicularly to the hill's ridgeline, a lateral enlargement of the fire front near the ridgeline occurs. McRae (2004) first noticed this phenomenon and designated it as 'fire channelling' or 'lee-slope channelling'. Sharples *et al.* (2012) has investigated the phenomena based on real-fire observations, where analysis of several possible mechanisms revealed that hill's lee-slope eddy plays a key role in driving the fire channelling process. The process is proposed to be a result of an interaction between the fire-induced convection (pyro-convection) and the terrain-modified winds through mechanisms that still needs to be investigated. An experimental study by (Raposo *et al.* 2015) was conducted on an isolated prismatic hill with horizontal ridgeline, and it demonstrated that the fire enlarges symmetrically on the two directions near the top of the crest

due to the interaction between fire and wind. Another extreme fire behaviour is commonly found happening over slopes and in canyons, which is the eruptive fire behaviour or the fire blow-up behaviour (Viegas 2006).

In the present paper, we analyse the fire behaviour over two prismatic hills placed in series in the direction of the wind. To avoid the effect of the Reynolds number on the location of flow separation we adopted a sharp ridgeline. This configuration is important to investigate considering that terrain-modified wind field is certainly different in the existence of other hills on the landscape, which in return will affect the fire behaviour as well. We gave particular attention to the lateral fire growth behaviour (fire channelling) over the lee-slopes and the fire behaviour between the two hills where an eruptive fire behaviour may take place. The study contributes to the understanding of the conditions where this extreme behaviour occurs and its characteristics. The investigation is made by performing a set of laboratory-scale experiments under various conditions of wind, slope and distances separating the hills

As the previously mentioned studies already indicated that the terrain-modified wind is playing an essential role on driving the fire behaviour over hills, we performed an analysis for the adiabatic flow in the absence of fire using computational fluid dynamics (CFD) simulations. However, we are presenting only the results that we consider relevant to interpret the fire behaviour over the hills. We are reporting the methodology used in both experimental and numerical analysis, followed by results then conclusions.

2. Methods and Materials

2.1. Hill Configuration and Terminology

The two hills have the same size and shape which is shown in Figure . Each hill is constructed from two rectangular faces with a non-identical width between the windward and leeward faces where they are scaled 3:2 (windward face width: leeward face width). The non-identical faces allow having a steeper lee slope. Also, the larger width of the windward allows the flow to accelerate over it. Through the presentation of our study, the two angles of the windward and leeward faces are referenced as α and β respectively measured from a horizontal reference. The distance between the two hills is designated as *D*. Also, we consider associating a number of 1 or 2 at the end of any parameter designation to identify that the parameter is associated to the first or second hill from the perspective of the wind direction. We designate the two lateral ends of the hill as the right end (*R*), and the left end (*L*), which are from a perspective of a person that stands facing the windward face of the hill and the wind is blowing from his back.

2.2. Experimental analysis setup

2.2.1. Physical Simulation

In the present study, the hills were covered by fuel and subjected to a surface fire that is originated from a single point. We, therefore, exclude spot and crown fires that may occur in a real fire.

The physical model had the dimensions shown in **Erro! A origem da referência não foi encontrada.**1. The hills faces are constructed from steel plates covered by a metallic grid to hold the fuel bed particles. The hill models were placed at the centre of the Combustion Wind Tunnel of the Forest Fire Research Laboratory of the University of Coimbra in Lousã (Portugal), where the midpoint of distance D is at the centre of the tunnel. The tunnel has an open working area of 6x8 m^2 with two lateral 2 m high walls but without ceiling (Figure). The flow is generated by two axial fans of 72kW that can produce a flow with maximum reference velocity of 7 m.s-1. The flow velocity is controlled by the rotational speed of the fans. Great care was taken to assure that the flow in the Combustion Tunnel is uniform across the test section (perpendicular to the flow). The flow over the floor of the

tunnel is of a boundary layer type with a reference velocity *Uo* that is measured at the centre of the working section floor and 0.5 m above the ground in the absence of the model. A rounded end body was built for each value of α and attached to the model of the first hill to produce a smooth flow around the hill ends as shown in Figure . This procedure was taken to reduce the end effects on the fire propagation over the hill and as well reducing the flow turbulence that affects the area between the two hills.

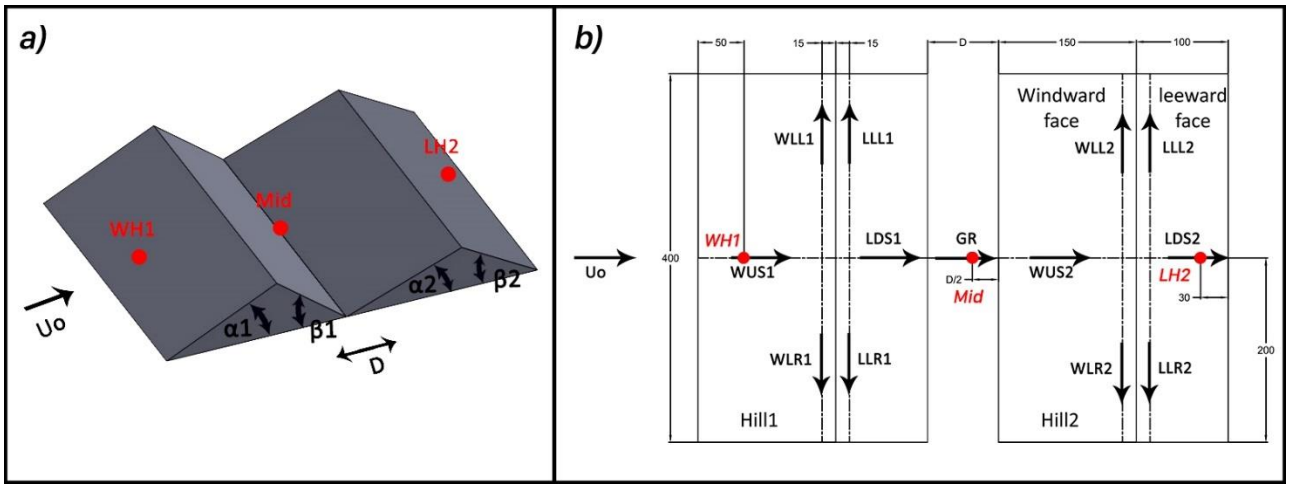

Figure 1 - a) Schematic view of the two triangular hills with the terminology configuration parameters b) Plan view of the used model size with the directions used to evaluate the ROS of the fire. The three ignition points that were used are labelled in* red*. The dimensions are indicated in cm.

The used α values in the fire spread experiments were 20º and 27º (**Erro! A origem da referência não foi encontrada.**a). Therefore the correspondent β values are ~ 31º and 43º respectively. The reason for choosing these angle values is to limit the slope angles in all cases to be not lower than 20º and not higher than 45º, which is the common range of hills' slope angles in the nature, also because (Sharples *et al.* 2012) determined that the fire channelling phenomena happens only within this range. The used *D* values are 0.5, 1, 1.5 and 2 m; in addition to no-distance (*D*=0), these four values correspond to about one to four times the height of the hill for α=20º, which is fixed inclination angle for all the tests where *D* was changed. The considered values of U_o are 0, 1, 2 and 3 m.s^{-1}. The fire was ignited at a point of three positions which are *WH1*, *LH2* or *Mid* (Figure), where *WH1* corresponds to the windward face of the first hill. *LH2* corresponds to the leeward face of the second hill, and *Mid* corresponds to the midpoint of the distance *D*. The three ignition points are at the mid-section of the hill (mid of the ridgeline) and in the cases of *WH1* and *LH2*, the ignition was made at a distance of 0.5m and 0.3m respectively measured over the face from the ground base. A combination of all these values of the parameters U_o, α, *D* and ignition positions was made taking into account fixing all parameters and change only one per group of tests. In total, 17 tests are presented on this paper where their parameters and designations are reported in Table . The test designations (references) will be used from now on referring to each test without ambiguity.

Figure 2 - Image showing the hill models placed in the wind combustion tunnel during one of the experiments, also attached the rounded ends to the left and right sides of the first hill is apparent

The hills' faces and the ground between the two hills if applicable were covered by a uniform fuel bed composed of dead pine needles (*Pinus Pinaster*) with a load of 0.6 $kg.m^{-2}$ (dry basis) and an average depth of 0.05 m. The used fuel has an average surface area to volume (SAV) ratio of ~ 2640 m^{-1}. The fuel moisture content was measured for each set of experiments with an A&D ML50 moisture analyser, and the amount of moisture was compensated to keep the fuel-loading constant on a dry basis. The range of values of the moisture content in the tests was 9%<mf<15.4% (dry basis). We define the set of experiments as a group of experiments performed on the same day while the change in moisture content does not exceed 5% during the testing time of the set.

For each set of experiments as well, we define a basic rate of spread (ROS) Ro which is determined by performing a reference test in no-wind and no-slope conditions. We used a flat 1m2 table with strings taut over the fuel bed and spaced 10 cm between them to perform the reference test. The time taken by the fire to pass from a string to another is measured. The basic ROS is defined as the slope of the linear fitting between the two data sets, time versus distance, following (Viegas 2004).

After the fire is ignited, the air flow was turned on to a pre-adjusted velocity. An IR camera was used to record the fire evolution. The obtained images (frames) from the IR recording were analysed using the open source software Fire ROS Calculator (Abouali 2017), which calibrates the camera and determines the ROS values along predefined directions by the user. We will not present further details about the program as it is not the main concern here. However, the program's outputs have been verified to have an error margin on its results of ± 5% (Abouali 2017).

2.2.2. Fire Spread Analysis

Using the above methodology, we obtain the fire contour evolution for each test and the ROS. To better interpret the properties of the fire spread, we define the following directions to estimate the ROS along them (Figure b):

WUS – Upslope over the windward face. This direction is along a line that is originated at the midpoint of the ridgeline and perpendicular to it over the windward face. This direction is shifted from

the middle of the ridgeline in some tests to follow the up-slope propagation of the fire as it didn't take place at the middle

LDS – Downslope over the leeward face. Along a collinear line to the *WUS* line but over the leeward face

WL – Lateral over the windward face. This direction is parallel to the ridgeline and at an average distance of 0.3 m from it. It starts from the middle of the ridgeline and ends at one of the ends. We designate the direction towards the right end as *WLR* and towards the left end as *WLL*. Also, we designate *WLA* to refer to the average between the two directions left and right.

LL – Lateral over the leeward face. The direction has the same remarks as on the *WL*, but it is over the leeward face and an average distance of 0.15 m from the ridgeline.

GR– Down-ridge over the windward face. This direction is collinear to the *WUS* and *WDS* but it is over the ground in the area between the two hills if *D*=0. In the case the ignition is at the *Mid* position, we designate *GRA* to refer to the average between the directions towards the first and the second hills along the same collinear line.

Considering two positions P_i and P_{i+1} of the fire front along a given direction at time t_i and t_{i+1} at distances d_i and d_{i+1} measured from the same reference we can determine the instantaneous value of the ROS as:

$$R(t) = \frac{d_{i+1} - d_i}{t_{i+1} - t_i}$$

Assuming that the fire spreads along the reference direction is steady, knowing the distances d_k of the fire front position at a set of times t_k (k=1…n), we can determine the average ROS ($\bar{R}$) of the fire along that direction by calculating the slope of the linear fitting between the two data sets (Viegas 2006). The time intervals (data samples) that were used to estimate the average ROS were determined for each direction on each test separately, but they meet the criteria of having at least four data samples and the time lapse is not less than 5 seconds or greater than 30 seconds.

Although in the general case the fire spread is not steady according to (Viegas 2004), we shall consider average values of the ROS along the six above mentioned directions like for example $\bar{R}_{WUR}$, $\bar{R}_{LLA}$. Given that our method of analysis can deal with many data points, this calculation was made for several close and parallel lines which represent one of the six indicated directions, to avoid local effects and to better characterize the average value of the ROS.

To guarantee the quality of the tests' results, we replicated all tests in two experiments, where the test replication was not performed on the same day to assure different conditions. We calculated a confidence interval (CI) for the determined average ROS values from the replicates in each direction and each test. The calculated CI is expressed as a percentage of the average of the same values used to calculate the CI (the ROS values). If the percentage was lower than 20% in all directions, the result is considered valid. In the opposite case, the test was replicated until the calculated percentage from any two tests was less than 20% in all six directions. However, for the ROS values that are close to the R_o, the validity condition is increased from 20% to 50%.

$$CI = NORMSINV * \frac{1 - alpha}{2} * \frac{sigma}{\sqrt{n}}$$

Where NORMSINV is a Microsoft Excel (2016) iterative function that returns the inverse of the standard normal cumulative distribution; alpha is taken by 0.05 for all the tests; sigma is the standard deviation based on the entire population (n), which is taken by two always as the CI is calculated between the results of two tests.

In order to minimise the effect of small variations of fuel bed properties, namely moisture content, following (Viegas and Neto 1991), we use the non-dimensional ROS (NDROS) (R') values given by:

$$R' = \frac{R}{R_o}$$

In this equation, R_o is the basic ROS measured in no-slope and no-wind conditions that were measured for each testing session.

We consider that the rate of spread is relatively low when R' is close to unity, but if it reaches values greater than 5 or if it increases rapidly then we consider that we are in the presence of an extreme behaviour (Viegas 2012).

2.3. Numerical Simulation Analysis Setup

2.3.1. The Model and Domain

A CFD simulation of the flow around the hills was performed using the open source CFD software OpenFOAM-5 (Weller *et al.* 1998). The adiabatic flow is simulated around a model that is similar to the experimental model but scaled down four times to not increase the size of the domain and therefore the required computational resources (The reported simulations are computed using in average 300 CPUcore and 1200 Gb of memory). The simulation was made for five configurations which correspond to tests 2D3, 2D14, 2D16, 2D23 and 2D24 (c.f. Table). On these configurations, the only parameter that was changed is the distance between the hills (*D*). We have chosen it that as this parameter is responsible for dramatic changes in the fire behaviour as we shall see on the discussion.

The dimensions of the simulation domain (Figure) consist of a box with dimensions of 2.0 m width (y-direction), 1.5 m height and the length (x-direction) of the domain was variable according to the configuration that is being simulated, where the hill's model is placed at a distance of 0.65m between the inlet section and the base windward face of the first hill, then the end of the domain was determined to be at ten times the height (10h) of the simulated hill measured from the end of the leeward face of the second hill (Figure). The choice of the end of the domain to be10h is based on the results of (Arya *et al.* 1981) where he estimated the reattachment point of the flow over the triangular ridge to be at 10 times the height of the hill.

The flow is assumed to be incompressible and adiabatic. The inlet flow is steady with a uniform velocity of 8.0 $m.s^{-1}$, which gives a Reynolds number based on the hill's height of the order of $6.5x10^4$ assuming constant flow temperature of 25º C. This velocity was chosen to have a flow's Reynolds number of the same order in both the simulations and experimental tests since the model sizes are different.

It is assumed that there is no flow across the lateral and the top boundaries of the domain (boundaries of a wall type). The flow near the ground is a boundary layer type developed upwind of the hill. Initially, the pressure is considered uniform and equal to 1 atmosphere in all the domain and velocity is zero.

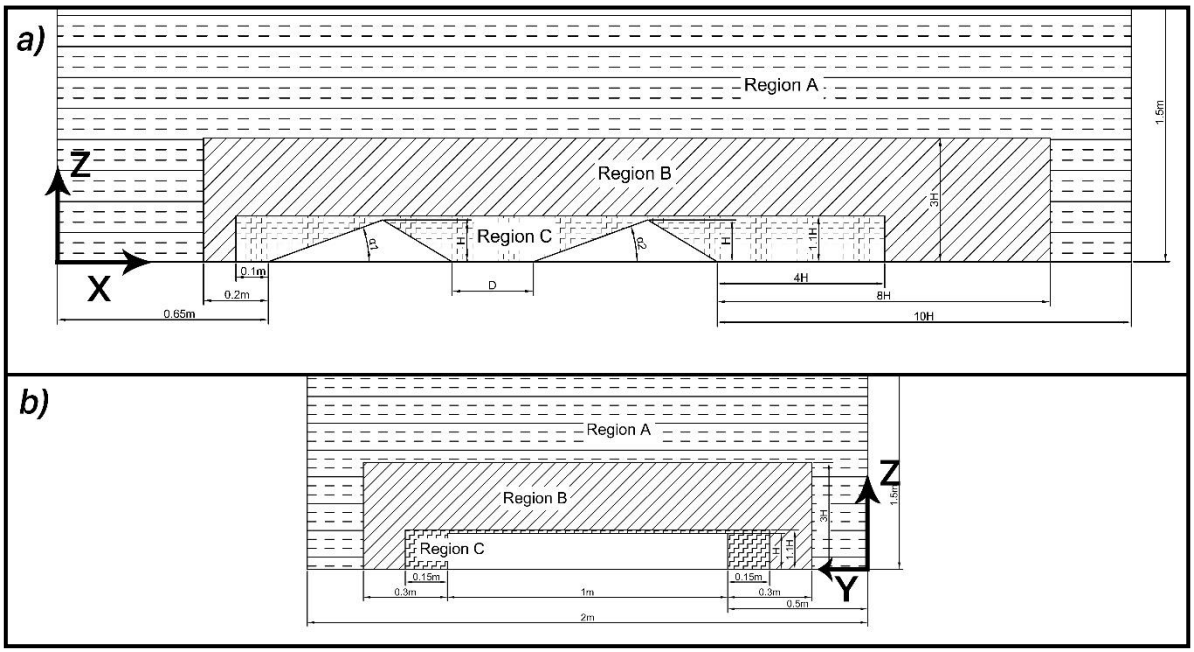

Figure 3 - Two cross sections on the calculation domain showing the axes directions, refinement regions with their dimensions and the position of the model a) parallel to the wind direction (x-z plane). b) perpendicular to the wind direction (y-z plane).

2.3.2. The Simulation Mesh

The mesh was created using the OpenFOAM tool SnappyHexMesh (Greenshields 2015). A course structured mesh with a cell size of 0.05m was built then refined and snapped to the model. The refinement is characterised by its level where level 1 corresponds to the coarsest mesh (0.05m), and then each refinement level has a cell size of the previous level divided by two (i.e. level 2 of refinement will have a cell size of 0.025m). We divided the domain into three regions A, B and C (Fig. 3) which have different levels of refinement. Region A coincides with the whole calculation domain and regions B and C are surrounding the model. Their heights (z-direction) equal to 3 and 1.1 times the height of the model respectively. Their widths (y-direction) are 1.3 and 1.15 times the width of the model respectively. The regions are centred with the model along the y-direction and their limits along the x-direction start at 0.2m and 0.1m measured from the base of the windward face of the first hill and ends at 8 and 4 times the height of the model measured from the base of the leeward face of the second hill. The three regions have refinement levels of 1, 3 and 4 respectively. Four transition refinement levels were configured between any two cells of different refinement levels whenever applicable to assure smooth transitions. The mesh then snapped to the model with refinement levels of 7 to 9 depending on the refinement needed for the snapping. Around the model's edges, the refinement was of level 9. Finally, 3 wall layers were added where the first layer attached to the model is of the thickness 8.5E-5m and the other two layers have a growth factor of 1.1 from one to another, this results in a Y+ value of ~1.9.

2.3.3. Turbulence model and convergence

We tested several meshes, turbulence models and solving algorithms. The presented results were obtained using the k-omega Shear Stress Transport (SST) turbulence model (Menter *et al.* 2003) and the SIMPLEC algorithm. The selection of these CFD parameters along with the mesh was made based on a convergence study where we compared the simulation results, namely the pressure at 90 different pressure tabs over the surfaces of the model against experimental results obtained at the same locations from wind tunnel experiments that we performed using the same model configuration and wind velocity. The reported results achieved convergence criteria composed of two factors that are satisfied,

which are a mean squared error less than 30% compared to the experimental measurements. The other factor is a residual error on the CFD solution less than 5E-4. However, the comparison against the experimentally obtained results was made only for the simulation of the configuration that corresponds to test 2D16 (c.f. Table), then the same setup was used to simulate the flow over the rest of the configurations.

We are not reporting the wind tunnel tests results or the setup for the sake of keeping the text focused on the most relevant results. However, we took on consideration the common procedures in performing such tests following (Tropea *et al.* 2007).

2.3.4. Obtaining the results

We focused the obtained results on the flow velocity near the surfaces of the model (0.1 m above the surface for all the results) considering its importance on driving the fire behaviour. We obtained the velocity and its components at points that are redistributed along three lines, which are the *middle line*, *quarter line* and *leeward line* (Figure). The *middle line* is a line that passes at the middle of the hills (middle of the ridgeline) and starts at the base of the windward face of the first hill and ends at the base of the second hill.

The *quarter line* is similar to the middle line but it passes at quarter of the ridgeline from the left side of the hill, we considered only the lift side as there is symmetry between the two sides in ideal flow conditions; the length of this line and the *middle line* are dependent on the configuration, namely the value of *D*. The *leeward line* is parallel to the ridgeline over the leeward face and spaced from it by 0.025m (10% of the face width).

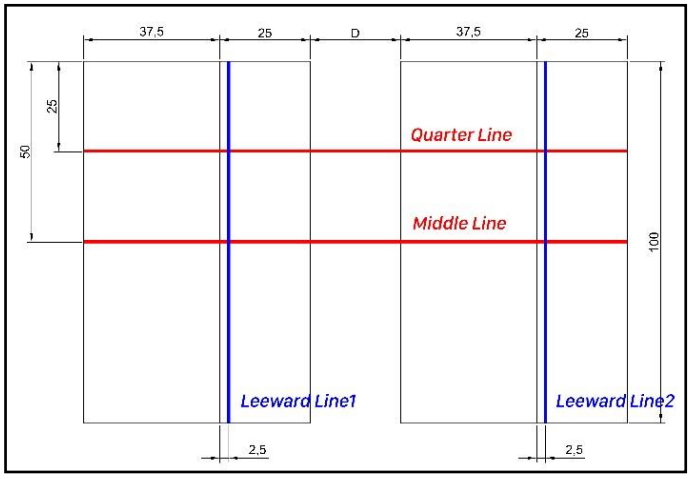

Figure 4 - a plane view showing the size of the model that was used in the simulation along with lines that the results (flow velocities) were obtained along them

3. Results and Discussion

3.1. Overall Fire Behaviour

In overall, the fire behaviour over the hills is dependent on their configuration, namely the slope; in addition to the blowing wind direction and velocity, and the approaching fire front direction and width. We performed two tests to analyse the fire behaviour in the absence of wind in order to better assess the role of the wind in driving the fire behaviour. On these two tests, 2D1 and 2D5, the two hills are configured to have equal α values, where we used the two values of α of 20º and 27º, one for each test. The tests revealed that the fire spreads with NDROS values that are close to 1 except in the WUS1&2 directions (Figure), where the spread was relatively faster as expected (Viegas 2006).

However, it's noticeable also that the spread on the WUS2 is faster than WUS1 (Table), which is due to the fact that the fire approaches the second hill with a wider fire front.

It is well known that the fire spreads faster up-slope as we increase the slope of a surface, and in the case of having a blowing wind on the same direction of the up-slope propagation, the fire propagates even faster proportionally to the blowing wind speed. This can easily be noticed on the reported NDROS of the fire in the *WUS1* direction in Table with all the tests where we had an ignition on *WH1*. However, over the upslope direction of the second hill (*WUS2*), the achieved ROS by the fire is different and it is affected by the recirculated flow between the two hills and the fire-induced flow. These flows also create the phenomena of the fire channelling. On the following two sections we discuss the fire channelling behaviour and the fire behaviour between the hills.

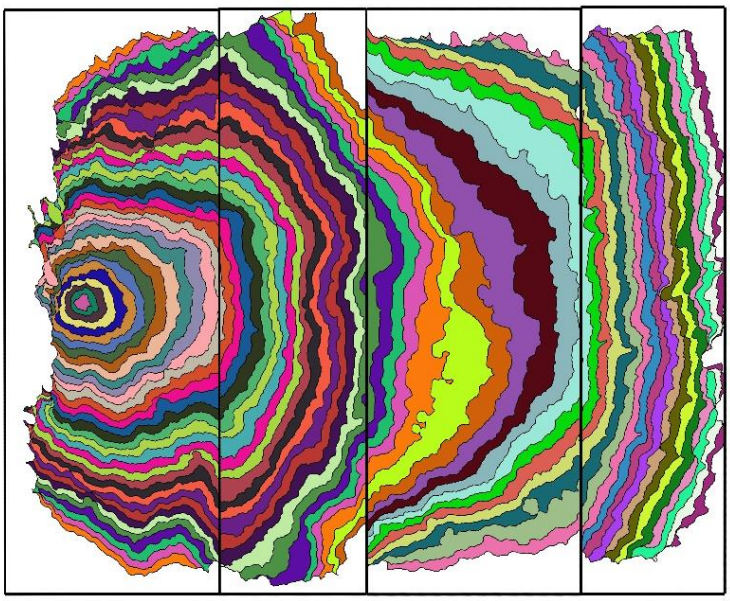

Figure 5 - Fire propagation contour map for test 2D1, showing the fire evolution over the hills in the absence of wind and with an $\alpha_1 = \alpha_2 = 20^o$. The time lapse between frames is 30 s.

Table 1 A list with the performed tests along with their parameters and the average NDROS of the fire along the predefined directions (Figure b) for each test

Test Ref.	U_o	$\alpha1,\alpha2$	Ignition	D	WUS1	WLA1	LDS1	LLA1	WUS2	WLA2	LDS2	LLA2	GRA
2D1	0	20,20	WH1	0	1.04	0.83	0.58	1.01	1.60	1.56	0.61	1.55	-
2D2	1				3.01	0.91	0.74	2.05	3.46	2.48	0.87	2.09	
2D3	2				8.34	0.98	0.76	2.53	4.53	1.85	1.26	2.84	
2D4	3				19.12	2.28	1.56	5.71	5.06	2.24	2.28	7.43	
2D5	0	27,27	WH1	0	1.76	1.25	0.99	1.32	3.45	1.78	0.84	1.70	-
2D6	1				4.21	1.09	1.08	2.95	3.78	1.70	1.02	2.62	
2D7	2				8.20	1.28	1.26	3.58	7.57	1.55	1.15	3.23	
2D8	3				14.63	1.48	1.42	4.56	7.24	1.47	1.00	3.72	
2D17	0	20,20	Mid	0	0.68	0.91	1.97	0.91	1.10	1.11	0.73	1.19	-
2D18	2				0.19	-	1.65	4.66	1.47	1.22	0.96	1.88	
2D19	0	20,20	LH2	0	0.84	3.14	4.14	3.30	0.75	1.06	1.71	0.96	-
2D20	2				0.28	-	3.98	9.64	0.64	0.47	1.54	3.73	
2D14	2	20,20	WH1	0.5	10.34	1.16	0.95	2.80	2.29	3.07	1.54	3.62	0.70
2D16				1	6.29	1.14	0.73	2.56	6.56	3.85	0.95	3.11	0.61
2D23				1.5	8.51	1.23	0.84	2.82	18.32	2.46	1.14	3.23	1.13
2D24				2	7.68	1.35	8.18	3.10	14.86	2.83	1.04	3.47	1.04
2D25	2	20,20	Mid	1	-	-	3.30	6.00	2.09	6.26	1.12	4.49	0.76

3.2. The fire channelling

In our tests, a lateral spread of the fire or the so called fire channelling happened always if *Uo*>0 over the leeward face of the first hill near the ridgeline regardless the fire front approaching direction, either from the windward face with the direction of the wind or from the leeward against the wind direction (Figure 6). Over the second hill, the channelling also happened but in some tests where the fire approached the second ridgeline with wide fire front that prevents the channelling behaviour from taking place due to the limited ridgeline length.

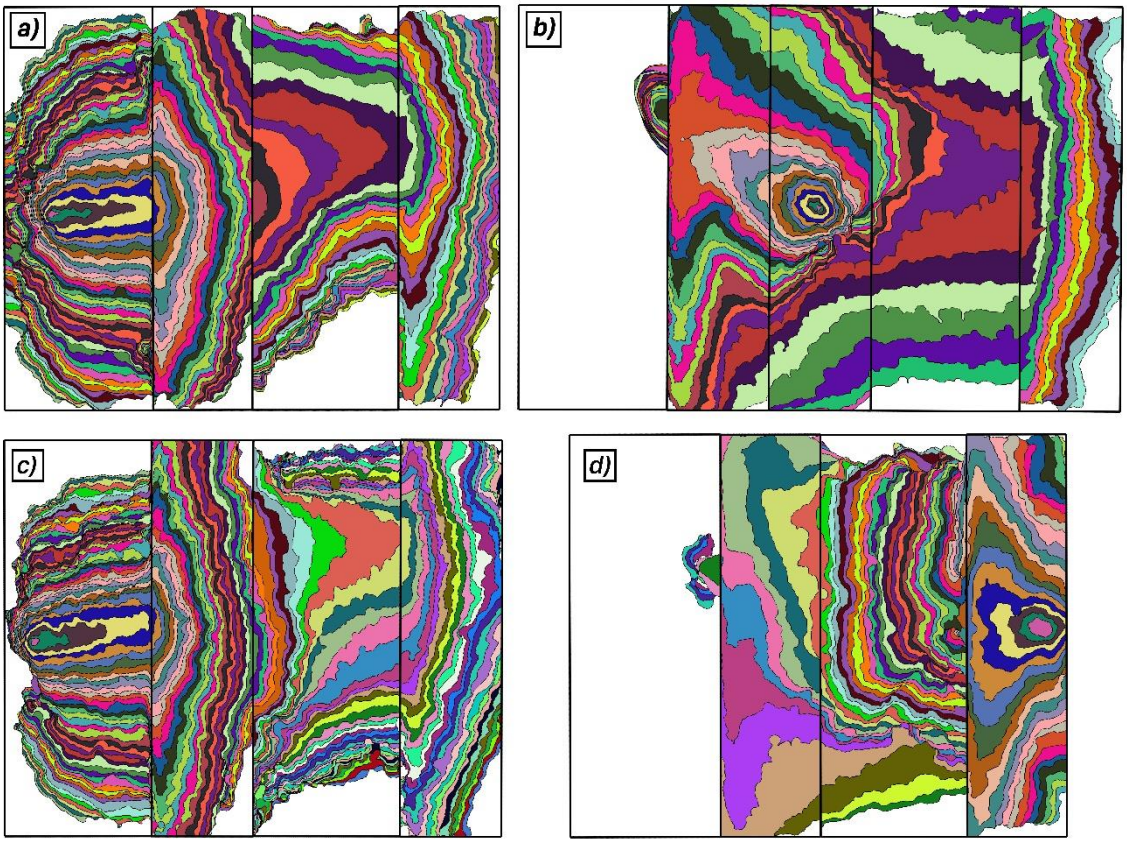

Figure 6 - Fire propagation contour maps showing the fire evolution over the hills in the presence of blowing wind with U_o=2 m.s-1 a) test 2D7 with α1= α2= 27º and D=0m. The time lapse between frames is 18 s. b) test 2D25 with α1= α2= 20º, D=1m and Mid ignition. The time lapse between frames is 20 s. c) test 2D3 with α1= α2= 20º and D=0m. The time lapse between frames is 15 s. d) test 2D20 with α1= α2= 20º, D=0m and LH2 ignition. The time lapse between frames is 30 s. The wind is blowing from left to right in all cases.

On Figure **Erro! A origem da referência não foi encontrada.** we plot the NDROS values of the fire on the LLA direction (the channelling direction) to illustrate the change on the behaviour with changing the distance between the hills (*D*) on (a) and the blowing wind velocity (U_o) on (b). We can notice that the fire spreads on this direction with similar ROS over the first and second hills for the same test in most of the cases regardless of the configuration except for the highest tested wind velocity U_o = 3 m.s^{-1}, where noticeably the fire spreads faster on the second hill than the first hill (Figure b). Also, we can find that the ROS of the fire is higher for higher inclination except for the case with U_o = 3 m.s^{-1}, where a sudden increase is evident in the lower inclination. By looking at the effect of changing *D* on the channelling behaviour (Figure a), we can notice that all the values are osculating around a NDROS value of 3 with small differences when we change the value of *D*. However, the channelling has a remarkably faster spread (almost the double) (Figure a) if the fire front approaches the leeward face of the hill from its base in the opposite direction to the blowing wind (Figure b), which is the case when we did a *Mid* ignition while *D*=1m. Also on another case when we had an

ignition at *LH2* (Figure d), the fire propagated even faster laterally over the first hill with a ROS that is around three times the lateral spread in case of igniting the fire at *WH1*(Figure a). This leads to an important remark that the fire channelling happens with faster ROS if the fire front approaches the hill from the leeward side in a contrary direction to the main stream compared to the approach from the windward side in the same direction of the wind.

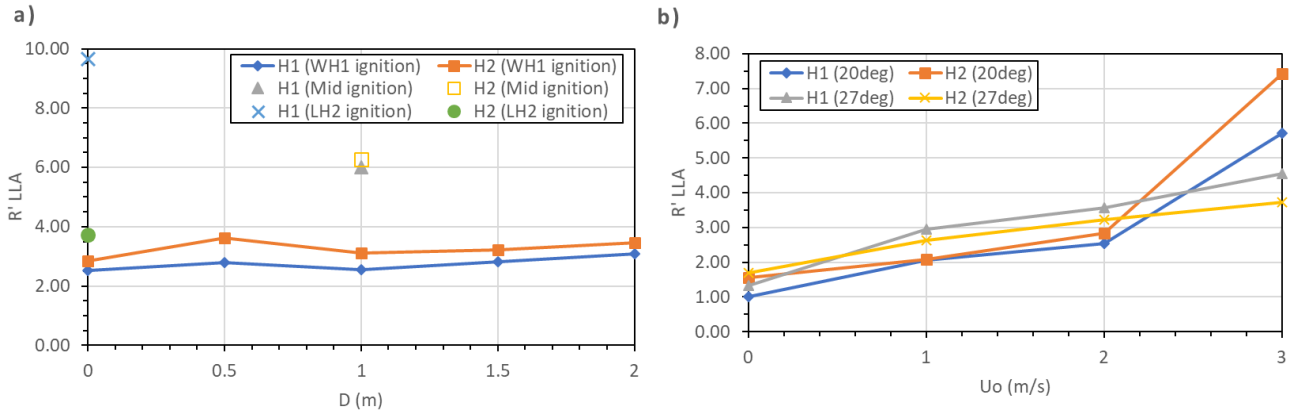

Figure 7 - The average NDROS (R') values of the fire propagation on the LLA1&2 directions plotted versus: a) the distance between the two hills (D) with different ignition points. b) the free stream velocity (U_o) with the two inclination scenarios, α1= α2= 20º and α1= α2= 27º

By looking at results of the adiabatic flow simulation (Figure), we can see a formation of two large eddies in the wake of both hills (between the two hills and after the second hill). The two eddies that are between the two hills are rotating in opposite directions, and they spread towards the middle of the hill where they spread after that in the x-direction above the second ridgeline where the flow exits the recirculation structure. These two formed eddies cause the flow to form patterns near the surface of the leeward face (Figure a) where the flow goes in an up-slope direction at the middle of the hill then rotates to be parallel to the ridgeline and goes towards the two ends of the hill. This flow pattern is the main driver of the fire channelling behaviour.

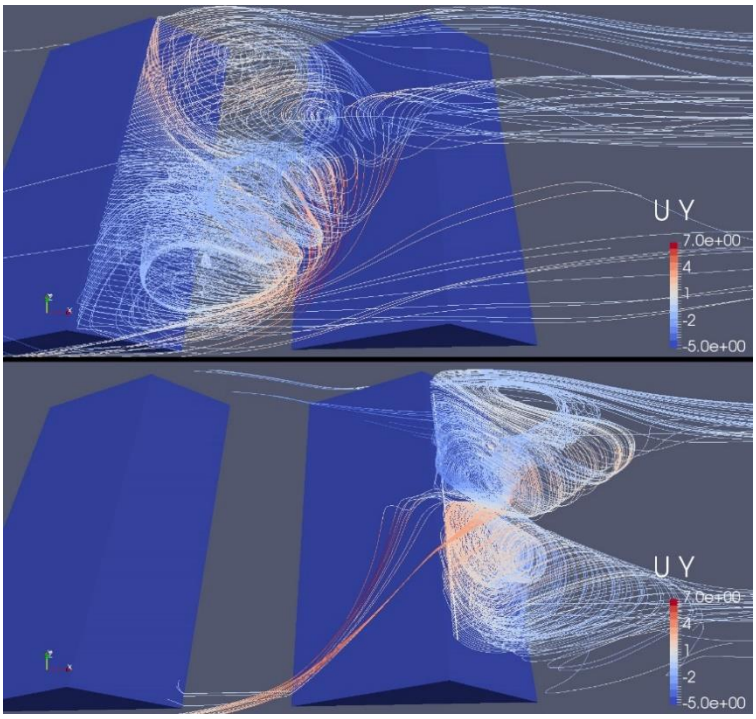

Figure 8 - Streamline of the flow in the wake of each of each of the two hills sources form a parallel line to the ridgeline (the leeward line) and coloured by the velocity y-component magnitude

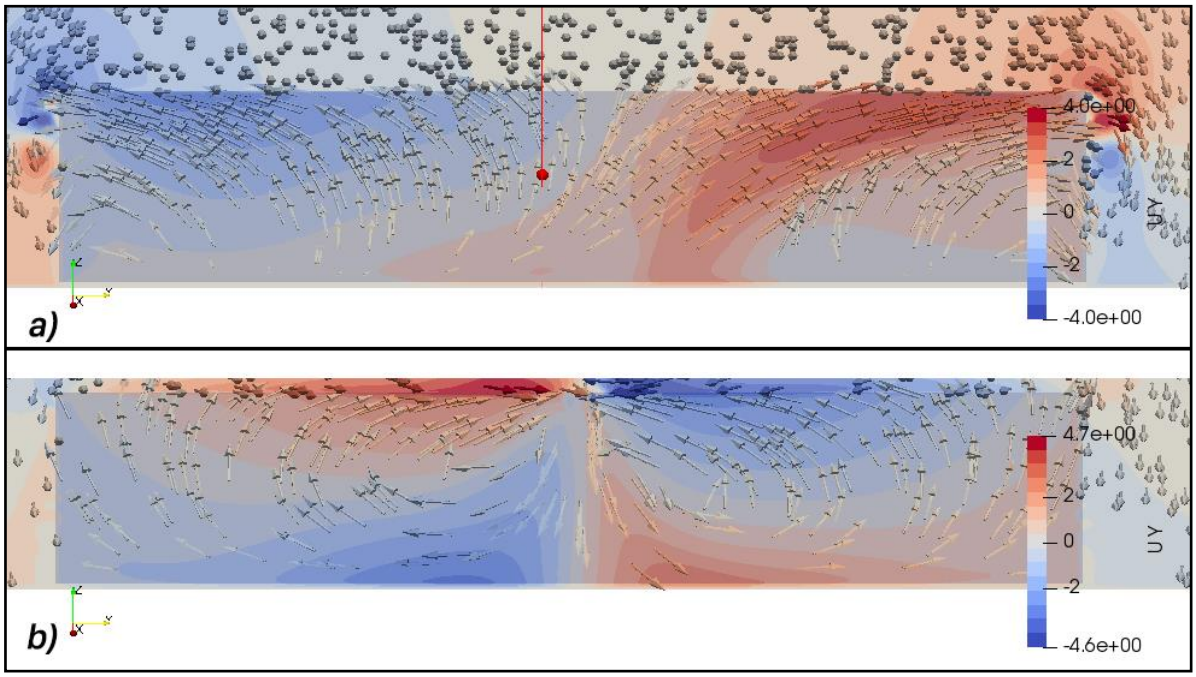

Figure 9 - Numerical results for the field of the velocity component in the y-direction (U_y) on parallel planes to the hills' leeward faces and spaced from them by 0.01m for the case where of D=0.25m along with the velocity vectors. a) The leeward of the first hill. b) The leeward of the second hill.

On Figure we report the values of the y-velocity component (U_y) that was computed for the adiabatic flow along the predefined line, the *leeward line*. The results show that the flow near the ridgeline of the first hill (Figure a) doesn't have a y-component velocity (U_y=0) at the middle of the hill, then a y-component starts to develop as we are heading towards the ends of the hill. However, over the second hill, the flow develops U_y also near the ridgeline but it has an opposite direction where the flow goes towards the middle of the hill not towards the ends (Figure b), which resulted from the rotating direction of the developed eddies in the wake of the second hill (Figure b). The adiabatic flow behaviour over near the surface of the first leeward coincides with the behaviour of the fire channelling, where we can find on Figure the instantaneous ROS of the lateral spread of the fire is increasing over the course of time (accelerating). But over the second hill, the fire tends to propagate with constant ROS over the course of time or even a deceleration behaviour. These two behaviours of lateral spread over the first and second hills can be easily related to the discussed behaviour of the local adiabatic flow (Figure). Taking into account the fire-induced flow, we can now interpret the remark that we addressed earlier about the faster lateral spread of the fire in the two ignition cases *Mid* and *LH2*, where the fire on this case was propagating on the same direction of the adiabatic flow towards up-slope at the middle of the hill (Figure a) then the lateral spread takes place near the ridgeline when the flow starts to develop a y-component velocity. During this scenario, the flow accelerates taking into account the fire-induced flow towards up-slope, which is not present if the fire was ignited at *WH1* and approached the ridgeline from the windward face (Figure a).

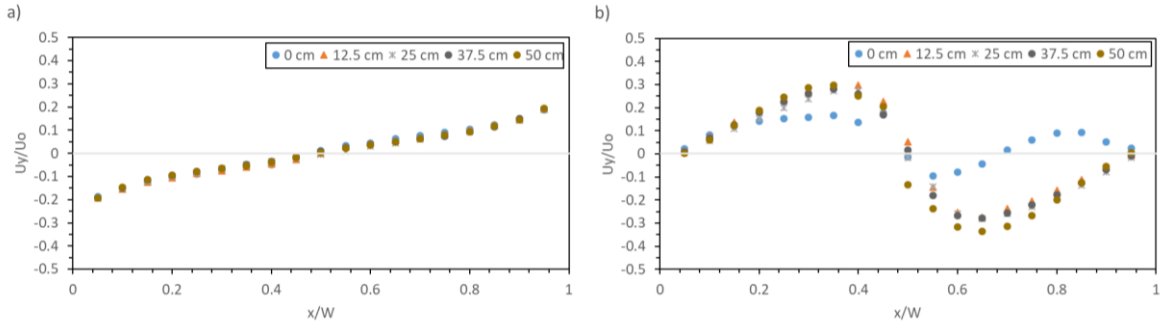

Figure 10 - Flow velocity results of the y-direction component (U_y) computed in the adiabatic flow simulation and obtained at points along a line parallel to the ridgeline and spaced from it by 0.025m (10% of the face width) and over the leeward face surface by 0.01m. a) over the first hill b) over the second hill. The velocity is presented dimensionless where the values are divided by the inlet flow stream velocity (U_o=8 m.s^{-1}). The x-axis represents the relative distance of the point compared to the ridgeline length (W), where zero corresponds to the right end of the hill and 1 is the left end.

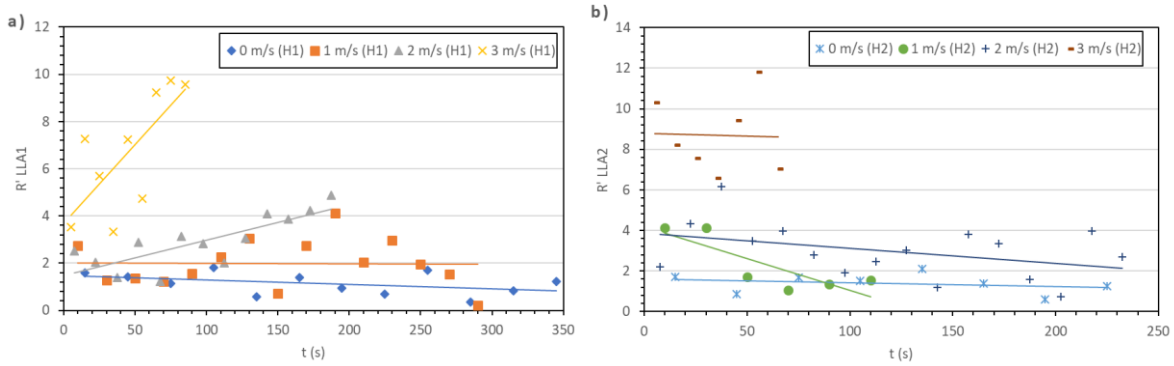

Figure 11 - The evolution of the instantaneous NDROS values over the time on LLA direction for different wind velocities (U_o) a) over the first hill (LLA1) b) over the second hill (LLA2).

1.2. The fire behaviour between the hills

We are focussing this section on the fire spread on *WUS2* and *GRA* directions, and the change of the fire behaviour along them with changing the distance between the two hills (*D*). On Figure b we can find that the fire's ROS on the up-slope direction increases as we increase the velocity (U_o), however, the increase is more evident on the *WUS1* than *WUS2*. Also, the *WUS1* is faster than WUS2 for all the tested wind velocities especially with high values of U_o where the difference can reach up to 4 times, all while *D*=0. But when we increase the value of *D*, we can notice on Figure a that there is a slight decrease in the ROS over the *WUS2* direction when *D*=0.5m then it increases as we increase *D* until we reach the case of *D*=1.5m, on these configurations we consider the eruptive fire behaviour is evident as the NDROS value is close to 18. For *D* values higher than 1.5m we can notice a slight decrease again. It's remarkable that at *D*=1m the ROS over *WUS1* and *WUS2* are matching. However, this matching doesn't necessarily lead to the conclusion that the fire has the same behaviour on the up-slope direction because the fire front is wider when approaching the second hill than it was on the first one (Figure).

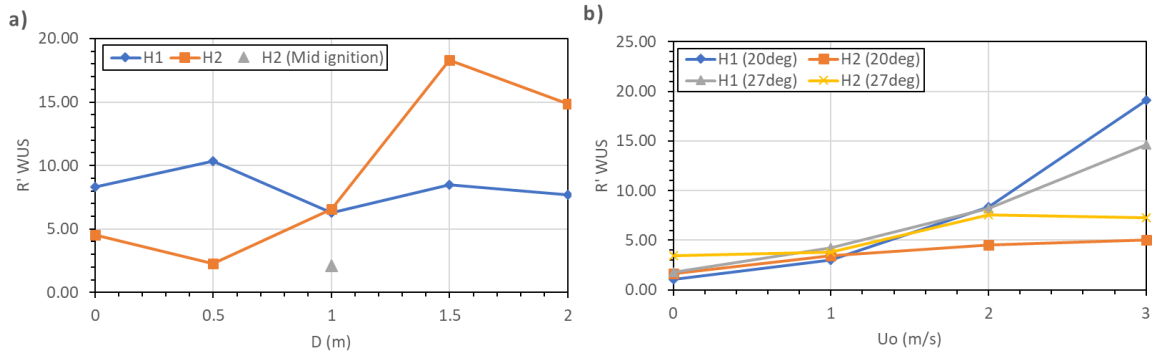

Figure 12 - The average NDROS (R') values of the fire propagation on the WUS1&2 directions plotted versus: a) the distance between the two hills (D) with different ignition points and U_o=2 m.s^{-1}, α1= α2= 20º. b) the free stream velocity (U_o) with the two inclination scenarios, α1= α2= 20º and α1= α2= 27º, and D=0.

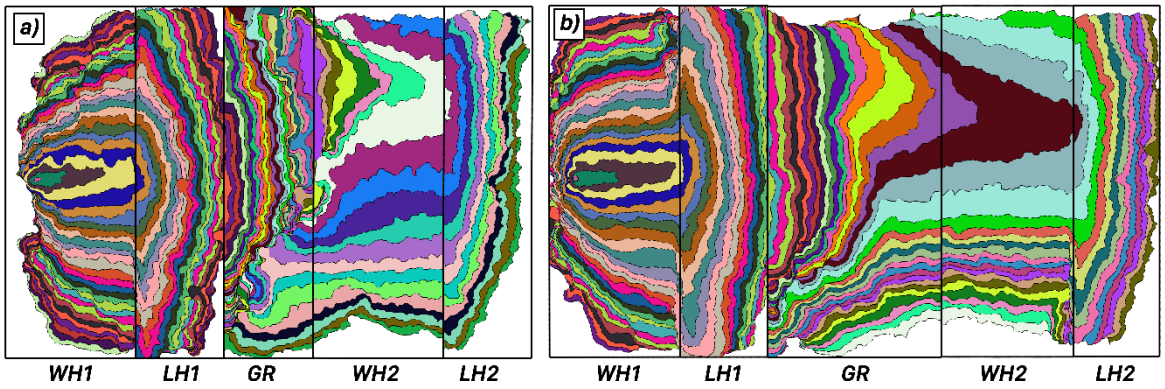

Figure 13 - Fire propagation contour maps showing the fire evolution over the hills in the presence of blowing wind with U_o=2 m.s-1 and α1= α2= 20º a) test 2D16 with D=1m. b) test 2D24with D=2m. The time lapse between frames is 30 s for both. The wind is blowing from left to right.

By looking at the results of the numerical solution of the adiabatic flow, we can find on Figure the flow velocity modulus values and the U_x and U_z components determined along the predefined *middle* and *quarter* lines (Figure). The one may notice that the flow near the windward surface of the second hill has lower velocities than the one of the first hill. This coincides with the observation that we obtained earlier about the fire spread on the upslope direction as the ROS is higher on *WUS1* compared to *WUS2*. Also, as we increase the distance between the hills (*D*), the near-surface flow velocities increase, which agree as well with the fire behaviour on the *WUS2* direction with increasing *D*. However, in most of our tests we noticed that the fire front approached the second windward from a point that's not at the middle but shifted towards the right or the left, as we can see on the tests that are presented on Figure and Figure , and on these cases the up-slope spread was shifted towards the left. This behaviour happens even if the fire front that is propagating on the ground reaches the middle of the hill first, as it's shown on Figure a, where the fire propagates very slowly towards up-slope until the fire reaches the left side of the windward face, then a fast up-slope (eruptive) propagation will develop.

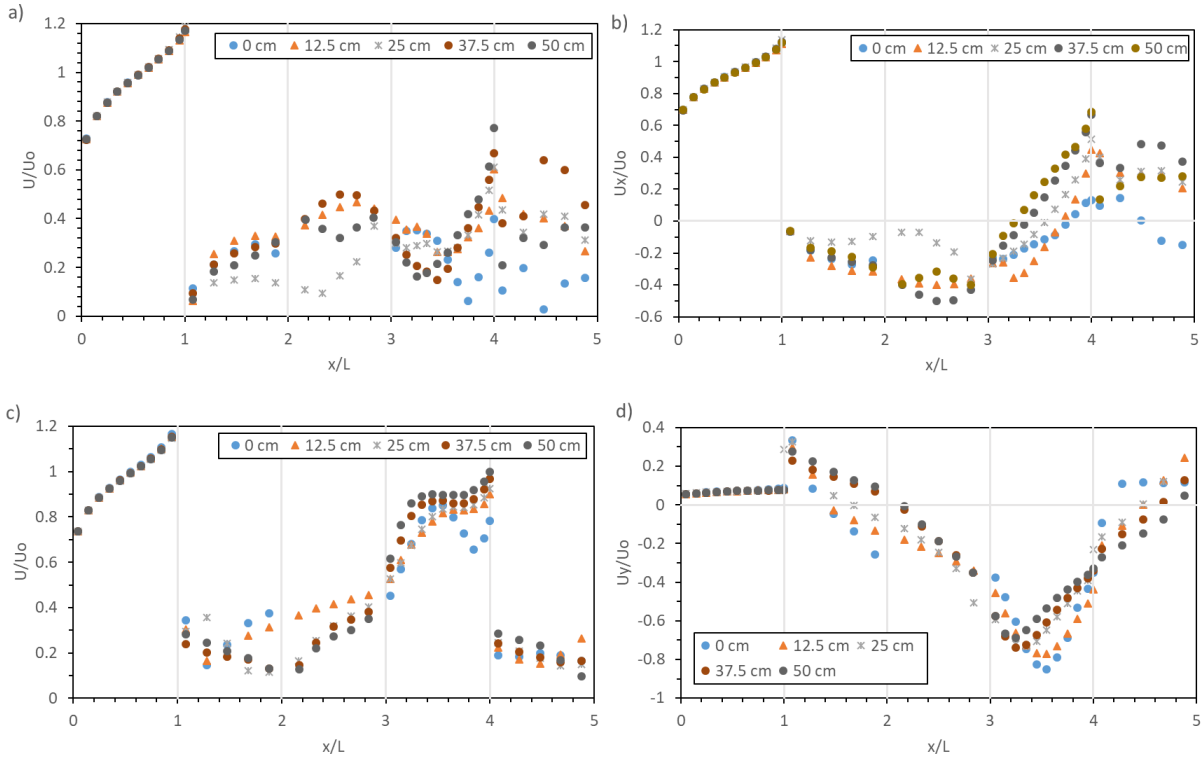

Figure 14 - Flow velocity results near the surface (1 cm) computed in the adiabatic flow simulation and obtained at points along two redefined lines at the middle an quarter of the hill where each line have a total length L. The velocity is presented dimensionless where the values are divided by the inlet flow stream velocity (U_o=8 m.s^{-1}). Each unit on the x-axis represents the width of each face, where from 0 to 1 is WH1 followed by LH1, GR, WH2 and LH2 respectively. a) velocity modulus along the middle line. b) velocity component in the x-direction (U_x) along the middle line. c) velocity modulus along the quarter line. d) velocity component in the y-direction (U_y) along the quarter line

By comparing the flow velocity modulus near the second windward surface along the *middle* line and the *quarter* line that are presented on Figure , we can realize that the flow has higher velocity along the quarter line than the middle line, in fact, along the middle the flow has a negative U_x values at the beginning of the of windward surface (Figure b), which means that the flow has an opposite direction to the up-slope fire spread direction. Meanwhile, along the quarter line, the flow has high transverse flow (U_y) with a direction towards the middle of the hill (Figure d). Furthermore, by looking at the flow topology that is presented by the streamlines on Figure , we can find that the two eddies that are formed between the hills are the ones that cause this flow pattern near the surface of the second windward face, which is presented on Figure , and we can see that there is a dead area at the middle of the hill with very low flow velocity and the velocity increases at the right and left from the middle.

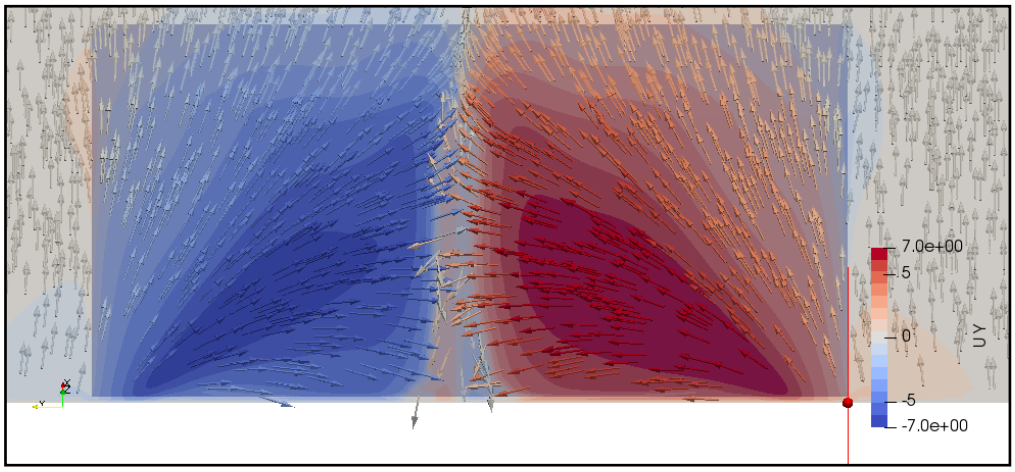

Figure 15 - Numerical results for the field of the velocity component in the y-direction (U_y) on a parallel plane to the second windward face and spaced from it by 0.01m for the case where of D=0.25m along with the velocity vectors.

The effect of the two circulation eddies is also evident on driving the fire behaviour on the ground (*GR*), where the flow near the ground surface is driven on the negative x-direction (Figure b) this results in a very slow propagation of the fire as we can find the values of the NDROS are close to 1 in the GR direction (Table). However, the negative U_x is apparent along the middle (Figure b), but along the quarter line, we can find that the flow over the gound has higher velocities with an increasing U_y as the flow gets closer to the second windward face (Figure d). This developed y-component of the flow drives the fire faster on the ground just before it reaches the second windward as we can see in Figure b.

From the mentioned observations about the adiabatic flow topology and patterns near the surface, we can conclude that the recirculated flow between the two hills has an apparent effect on driving the fire on the ground and the second windward face. It is noticeable also that the fire propagates in the same direction of the highest local flow velocity and enhance it by the fire-induced flow resulting in a fire propagation that is different from the typical up-slope spread (i.e. In the case that there are no obstacles before it in the direction of the wind), like the first windward in our configuration here.

4. Conclusion

The experiments discussed in this study explore the wildfire behaviour over two triangular hills placed on series in the direction of the wind with different configurations and applied wind velocities. We observed that the fire propagates laterally over the leeward faces of the hills near the ridgeline (fire channelling), these lateral spreads are noticeably faster if we increase the freestream velocity while the change in the fire's rate of spread with the change in the inclination of the hills or the distance between them is relatively small. Also, the lateral spread is remarkably faster on the first hill in the direction of wind than on the hill that has a topographic obstacle before it (the second hill in our study).

Based on the numerical simulations of the adiabatic flow we found that the topology of the recirculated flow in the wake of the hill is the principal cause of the lateral fire spread. The flow near the ridgeline where the fire channelling takes place has a lateral component with a value that can reach up to half of the freestream velocity value. Also, the lateral flow accelerates toward the hill sides, which coincides with the noticed accelerating fire spread behaviour from the middle of the hill towards the sides.

We also noticed that the fire channelling is faster (up to double) if the fire propagated over the leeward face towards up-slope in a contrary direction of the mainstream compared to the fire that propagates up-slope over the windward in the same direction of the mainstream. We rely this on the fire-induced flow as the up-slope propagation over the leeward face has the same direction as the local

terrain-modified flow, therefore, the fire enhances the flow velocity locally and feeds the fire channelling

Another remarkable fire behaviour explored as well was the spread of the fire over the windward face of the second hill in the direction of the wind. The up-slope spread over this face is generally slower than the spread rate in the similar direction (up-slope) over the first hill. This is clearer with high blowing wind velocities, and without having space between the two hills, in this case, the fire's rate of spread can be up to three times slower than the spread over the first hill. However, this slower rate of spread of the fire fades if we increased the distance between the two hills, in fact, with distances higher than two times the height of the hill, the fire propagates faster over the second windward in comparison with the first one. Furthermore, we noticed that the fire's propagation towards up-slope over the second windward is shifted from the middle towards one of the sides regardless of the fire's approaching point to the windward face.

We related the behaviour of the fire in the up-slope direction over the second windward with the topology of the recirculating flow between the two hills and the local adiabatic flow velocities, where we found that the same recirculation eddies that are responsible about the fire channelling are also responsible about shifting the up slope propagation over the second windward. Additionally, this reticulated flow causes the fire to propagate on the ground between the two hills relatively slow.

From these observations and conclusions, we can summarize that the terrain-modified flow has a significant effect on driving the fire over complex topographic terrains. Our results also show the importance of simulating the flow field over these terrains with high accuracy in order to better predict the fire growth.

5. Acknowledgements

The authors wish to thank the Portuguese Science Foundation for the support through the project for the project "FIREWHIRL – Vorticity Effects in Forest Fires" (PTDC/EMS-ENE/2530/2014). The authors are grateful to ADAI's team, namely Nuno Luis, António Cardoso and Eduardo Melo for their help to carry on the fire investigation tests. The authors also acknowledge the Laboratory for Advanced Computing at the University of Coimbra (www.lca.uc.pt) for providing {HPC, computing, consulting} resources that have contributed to the research results reported within this paper and the team of the laboratory, namely Professor Pedro Vieira Alberto.

6. References

Abouali A (2017) Fire ROS Calculator. doi:10.5281/ZENODO.898160.

Arya SPS, Shipman MS, Courtney LY (1981) An experimental investigation of flow and diffusion in the disturbed boundary layer over a ridge-II. Diffusion from a continuous point source. *Atmospheric Environment (1967)* **15**, 1185–1194. doi:10.1016/0004-6981(81)90309-7.

Greenshields C (2015) SnappyHexMesh. *OpenFOAM v4 User Guid.* https://cfd.direct/openfoam/user-guide/v4-snappyHexMesh/.

McRae RHD (2004) Breath of the dragon – observations of the January 2003 ACT Bushfires. *In: Proceedings of 2004 Australasian Bushfire Research Conference, May 2004, Adelaide*.

Menter FR, Kuntz M, Langtry R (2003) Ten Years of Industrial Experience with the SST Turbulence Model. *Turbulence Heat and Mass Transfer 4* **4**, 625–632. doi:10.4028/www.scientific.net/AMR.576.60.

Raposo JR, Cabiddu S, Viegas DX, Salis M, Sharples J (2015) Experimental analysis of fire spread across a two-dimensional ridge under wind conditions. *International Journal of Wildland Fire* **24**, 1008–1022. doi:10.1071/WF14150.

Sharples JJ, McRae RHD, Wilkes SR (2012) Wind-terrain effects on the propagation of wildfires in rugged terrain: Fire channelling. *International Journal of Wildland Fire* **21**, 282–296. doi:10.1071/WF10055.

Tropea C, Yarin AL, Foss JF (2007) 'Springer Handbook of Experimental Fluid Mechanics.' doi:10.1007/978-3-540-30299-5.

Viegas DX (2004) Slope and wind effects on fire propagation. *International Journal of Wildland Fire* **13**, 143–156. doi:10.1071/WF03046.

Viegas DX (2006) Parametric study of an eruptive fire behaviour model. *International Journal of Wildland Fire* **15**, 169–177. doi:10.1071/WF05050.

Viegas DX (2012) Extreme Fire Behaviour. 'For. Manag. Technol. Pract. Impact'. (Eds ACB Cruz, REG Correa) pp. 1–56. (Nova Science Publishers, Inc.: New York)

Viegas DX, Neto LPC (1991) Wall shear-stress as a parameter to correlate the rate of spread of a wind induced forest fire. *International Journal of Wildland Fire* **1**, 177–188. doi:10.1071/WF9910177.

Weller HG, Tabor G, Jasak H, Fureby C (1998) A tensorial approach to computational continuum mechanics using object-oriented techniques. *Computers in Physics* **12**, 620. doi:10.1063/1.168744.